Research Article | Vol. 26, No. 14 | 9 Jul 2018 | OPTICS EXPRESS 17899
Optics EXPRESS

Bridged-bowtie and cross bridged-bowtie nanohole arrays as SERS substrates with hotspot tunability and multi-wavelength SERS response

NITIN GUPTA AND ANUJ DHAWAN*

Department of Electrical Engineering, Indian Institute of Technology Delhi, Hauz Khas, New Delhi 110016, India
**adhawan@ee.iitd.ac.in*

Abstract: In this paper, we present bridged-bowtie nanohole arrays and cross bridged-bowtie nanohole arrays in a gold thin film as surface enhanced Raman scattering (SERS) substrates. These SERS substrates not only exhibit large electromagnetic enhancement of SERS but also have the SERS enhancement spread over a much larger area than what could be present in SERS substrates consisting of nanopillar arrays or nanopillar plasmonic nanoantennas. Numerical simulations based on the finite difference time domain (FDTD) method are employed to determine electric field enhancement factors (EFs) and therefore the electromagnetic SERS enhancement factor for these SERS substrates. It was observed that bridged-bowtie nanohole arrays and cross bridge-bowtie nanohole arrays exhibit a highest electromagnetic SERS enhancement factor (EF) of ~10^9, which is orders of magnitude higher than what has been previously reported for nanohole arrays as SERS substrates. This electromagnetic SERS EF (of ~10^9) is spread over a hotspot region of ~100 nm^2 (in each periodic unit of the array), which is larger than the case of nanopillar arrays. In addition, it was observed that an electromagnetic SERS enhancement factor of at least 10^8 is spread over a large area (500 nm^2 in each periodic unit of the array), thus increasing the average enhancement factor. It was observed that the bridged-bowtie nanohole arrays and the cross bridged-bowtie nanohole arrays can be employed as effective SERS substrates in both the transmission mode and the reflection mode. The resonance wavelength of these arrays of nanoholes can be tuned by altering the size of the nanoholes. The effects of varying the gold film thickness and the diameter of the bridged-bowtie nanoholes forming the arrays were also analyzed. The bridged-bowtie nanohole arrays and cross bridged-bowtie nanohole arrays exhibit very high electric field enhancement factors (EFs) at more than one wavelength, and can therefore be used to obtain a multi-wavelength SERS response. Moreover, the cross bridged-bowtie nanohole array allows the tunability of the position of the hotspot with the rotation of the direction of the polarization of incident field.

OCIS codes: (240.6680) Surface plasmons; (240.6695) Surface-enhanced Raman scattering; (170.5660) Raman spectroscopy; (310.6628) Subwavelength structures, nanostructures; (250.5403) Plasmonics; (220.4241) Nanostructure fabrication.

References and links

1. J. Kneipp, H. Kneipp, and K. Kneipp, "SERS-a single-molecule and nanoscale tool for bioanalytics," Chem. Soc. Rev. **37**(5), 1052–1060 (2008).
2. W. E. Doering and S. Nie, "Single-molecule and single-nanoparticle SERS: Examining the roles of surface active sites and chemical enhancement," J. Phys. Chem. B **106**(2), 311–317 (2002).
3. A. Campion, J. E. Ivanecky, C. M. Child, and M. Foster, "On the Mechanism of Chemical Enhancement in Surface-Enhanced Raman Scattering," J. Am. Chem. Soc. **117**(47), 11807–11808 (1995).
4. M. Kerker, "Electromagnetic Model for Surface-Enhanced Raman Scattering (SERS) on Metal Colloids," Acc. Chem. Res. **17**(8), 271–277 (1984).
5. S. Schlucker, *Surface Enhanced Raman Spectroscopy Analytical, Biophysical and Life Science Applications* (Wiley-VCH Verlag, 2011).

#319041 https://doi.org/10.1364/OE.26.017899
Journal © 2018 Received 23 Jan 2018; revised 2 Mar 2018; accepted 22 Mar 2018; published 27 Jun 2018

Optics EXPRESS

6. P.F. Liao, J.G. Bergman, D.S. Chemla, A. Wokaun, J. Melngailis, A.M. Hawryluk, and N.P. Economou, "Surface-enhanced Raman scattering from microlithographic silver particle surfaces," Chem. Phys. Lett. **82**(2), 1–5 (1981).
7. D. A. Weitz, S. Garoff, and T. J. Gramila, "Excitation spectra of surface-enhanced Raman scattering on silver-island films," Opt. Lett. **7**(4), 168–170 (1982).
8. T. Vo-Dinh, A. Dhawan, S. J. Norton, C. G. Khoury, H. N. Wang, V. Misra, and M. D. Gerhold, "Plasmonic nanoparticles and nanowires: Design, fabrication and application in sensing," J Phys Chem C Nanomater Interfaces **114**(16), 7480–7488 (2010).
9. S. J. Lee, A. R. Morrill, and M. Moskovits, "Hot spots in silver nanowire bundles for surface-enhanced Raman spectroscopy," J. Am. Chem. Soc. **128**(7), 2200–2201 (2006).
10. Y. Sharma and A. Dhawan, "Plasmonic "nano-fingers on nanowires" as SERS substrates," Opt. Lett. **41**(9), 2085–2088 (2016).
11. C. J. Orendorff, A. Gole, T. K. Sau, and C. J. Murphy, "Surface-enhanced Raman spectroscopy of self-assembled monolayers: Sandwich architecture and nanoparticle shape dependence," Anal. Chem. **77**(10), 3261–3266 (2005).
12. A. M. Jubb, Y. Jiao, G. Eres, S. T. Retterer, and B. Gu, "Elevated gold ellipse nanoantenna dimers as sensitive and tunable surface enhanced Raman spectroscopy substrates," Nanoscale **8**(10), 5641–5648 (2016).
13. M. G. Banaee and K. B. Crozier, "Gold nanorings as substrates for surface-enhanced Raman scattering," Opt. Lett. **35**(5), 760–762 (2010).
14. Y. Sharma and A. Dhawan, "Hybrid nanoparticle-nanoline plasmonic cavities as SERS substrates with gap-controlled enhancements and resonances," Nanotechnology **25**(8), 085202 (2014).
15. T. W. Ebbesen, H. J. Lezec, H. F. Ghaemi, T. Thio, P. A. Wolff, T. Thio, and P. A. Wolff, "Extraordinary optical transmission through sub-wavelength hole arrays," Nature **86**(6), 1114–1117 (1998).
16. L. Martín-Moreno, F. J. García-Vidal, H. J. Lezec, K. M. Pellerin, T. Thio, J. B. Pendry, and T. W. Ebbesen, "Theory of extraordinary optical transmission through subwavelength hole arrays," Phys. Rev. Lett. **86**(6), 1114–1117 (2001).
17. W. L. Barnes, A. Dereux, and T. W. Ebbesen, "Surface plasmon subwavelength optics," Nature **424**(6950), 824–830 (2003).
18. K. L. Van Der Molen, K. J. Klein Koerkamp, S. Enoch, F. B. Segerink, N. F. Van Hulst, and L. Kuipers, "Role of shape and localized resonances in extraordinary transmission through periodic arrays of subwavelength holes: Experiment and theory," Phys. Rev. B – Condens. Matter Mater. Phys. **72**(4), 1–9 (2005).
19. A. Degiron and T. W. Ebbesen, "The role of localized surface plasmon modes in the enhanced transmission of periodic subwavelength apertures," J. Opt. A, Pure Appl. Opt. **7**(2), S90–S96 (2005).
20. Z. Ruan and M. Qiu, "Enhanced transmission through periodic arrays of subwavelength holes: The role of localized waveguide resonances," Phys. Rev. Lett. **96**(23), 233901 (2006).
21. A. G. Brolo, E. Arctander, R. Gordon, B. Leathem, and K. L. Kavanagh, "Nanohole-enhanced raman scattering," Nano Lett. **4**(10), 2015–2018 (2004).
22. A. Lesuffleur, L. K. S. Kumar, A. G. Brolo, K. L. Kavanagh, and R. Gordon, "Apex-enhanced Raman spectroscopy using double-hole arrays in a gold film," J. Phys. Chem. C **111**(6), 2347–2350 (2007).
23. G. F. S. Andrade, J. G. Hayashi, M. M. Rahman, W. J. Salcedo, C. M. B. Cordeiro, and A. G. Brolo, "Surface-Enhanced Resonance Raman Scattering (SERRS) Using Au Nanohole Arrays on Optical Fiber Tips," Plasmonics **8**(2), 1113–1121 (2013).
24. A. Mahigir, T. W. Chang, A. Behnam, G. L. Liu, M. R. Gartia, and G. Veronis, "Plasmonic nanohole array for enhancing the SERS signal of a single layer of graphene in water," Sci. Rep. **7**(1), 14044 (2017).
25. S. Lal, N. K. Grady, J. Kundu, C. S. Levin, J. B. Lassiter, and N. J. Halas, "Tailoring plasmonic substrates for surface enhanced spectroscopies," Chem. Soc. Rev. **37**(5), 898–911 (2008).
26. S. Nikitin, S. Prokes, H. Qi, O. Glembocki, and J. Grun, "Multi-wavelength surface-enhanced Raman scattering from molecules adsorbed on plasmonic nanowires," in *Quantum Electronics and Laser Science Conference*, 2012 OSA Technical Digest Series (Optical Society of America, 2012), paper QTh4F.8.
27. M. Khanafer, I. Izquierdo-Lorenzo, S. Akil, G. Louarn, J. Toufaily, T. Hamieh, P.-M. Adam, and S. Jradi, "Silver Nanoparticle Rings of Controllable Size: Multi-Wavelength SERS Response and High Enhancement of Three Pyridine Derivatives," ChemistrySelect **1**(6), 1201–1206 (2016).
28. E. D. Palik, *Handbook of Optical Constants of Solids* (Academic, 1985).
29. Q. Li, Z. Yang, B. Ren, H. Xu, and Z. Tian, "The Relationship Between Extraordinary Optical Transmission and Surface-Enhanced Raman Scattering in Subwavelength Metallic Nanohole Arrays," J. Nanosci. Nanotechnol. **10**(11), 7188–7191 (2010).
30. Z.-L. Yang, Q.-H. Li, B. Ren, and Z.-Q. Tian, "Tunable SERS from aluminium nanohole arrays in the ultraviolet region," Chem. Commun. (Camb.) **47**(13), 3909–3911 (2011).
31. K. L. Van der Molen, F. B. Segerink, N. F. Van Hulst, and L. Kuipers, "Influence of hole size on the extraordinary transmission through subwavelength hole arrays," Appl. Phys. Lett. **85**(19), 4316–4318 (2004).
32. T. Thio, H. F. Ghaemi, H. J. Lezec, P. A. Wolff, and T. W. Ebbesen, "Surface-plasmon-enhanced transmission through hole arrays in Cr films," J. Opt. Soc. Am. B **16**(10), 1743 (1999).
33. Q. Fu, Z. Zhan, J. Dou, X. Zheng, R. Xu, M. Wu, and Y. Lei, "Highly Reproducible and Sensitive SERS Substrates with Ag Inter-Nanoparticle Gaps of 5 nm Fabricated by Ultrathin Aluminum Mask Technique," ACS Appl. Mater. Interfaces **7**(24), 13322–13328 (2015).

Optics EXPRESS

34. S. Jiang, J. Guo, C. Zhang, C. Li, M. Wang, Z. Li, S. Gao, P. Chen, H. Si, and S. Xu, "A sensitive, uniform, reproducible and stable SERS substrate has been presented based on MoS_2 @Ag nanoparticles@pyramidal silicon," RSC Advances **7**(10), 5764–5773 (2017).
35. A. Degiron, H. J. Lezec, W. L. Barnes, and T. W. Ebbesen, "Effects of hole depth on enhanced light transmission through subwavelength hole arrays," Appl. Phys. Lett. **81**(23), 4327–4329 (2002).
36. M. G. Stanford, B. B. Lewis, K. Mahady, J. D. Fowlkes, and P. D. Rack, "Review Article: Advanced nanoscale patterning and material synthesis with gas field helium and neon ion beams," J. Vac. Sci. Technol. B, Nanotechnol. and Microelectron. Mater. Process. Meas. Phenom. **35**(3), 30802 (2017).
37. M. Melli, A. Polyakov, D. Gargas, C. Huynh, L. Scipioni, W. Bao, D. F. Ogletree, P. J. Schuck, S. Cabrini, and A. Weber-Bargioni, "Reaching the theoretical resonance quality factor limit in coaxial plasmonic nanoresonators fabricated by helium ion lithography," Nano Lett. **13**(6), 2687–2691 (2013).
38. A. Dhawan, M. D. Gerhold, and J. F. Muth, "Plasmonic Structures Based on Subwavelength Apertures for Chemical and Biological Sensing Applications," IEEE Sens. J. **8**(6), 942–950 (2008).
39. M. Najiminaini, F. Vasefi, B. Kaminska, and J. J. L. Carson, "Nanohole-array-based device for 2D snapshot multispectral imaging," Sci. Rep. **3**(1), 2589 (2013).
40. M. D. Fischbein and M. Drndić, "Sub-10 nm device fabrication in a transmission electron microscope," Nano Lett. **7**(5), 1329–1337 (2007).

1. Introduction

Raman spectroscopy is a powerful noninvasive tool for identification of various molecules such as biomolecules, pesticides, chemical warfare agents, explosives, and pharmaceuticals. As the Raman cross-section of molecules is very small (it is of the order of 10^{-30} to 10^{-25} cm^2 per molecule), it is necessary to enhance the Raman signals to employ Raman spectroscopy for detection of trace amounts of molecules of interest [1].

Surface enhanced Raman scattering (SERS) has emerged as a powerful method that employs plasmonic nanostructures to enhance the Raman signals from molecules (lying in the vicinity of the nanostructures) by a factor ranging from 10^6 to 10^{12} as compared to the Raman signals in the absence of plasmonic nanostructures [2–4]. The enhancement of the Raman signals is mainly contributed by the two phenomena known as electromagnetic enhancement and chemical enhancement. Electromagnetic enhancement occurs due to the excitation of plasmon resonances in the plasmonic nanostructures or in metallic thin films. The electromagnetic field intensities are significantly enhanced at both the incident frequency as well as the Stokes frequency. As the Stokes frequency shift is very small compared to the incident frequency the total enhancement factor can be approximated to $|\mathbf{E}|^4/|\mathbf{E}_0|^4$ [5], where $|\mathbf{E}_0|$ is the magnitude of the incident electric field and $|\mathbf{E}|$ is the magnitude of the electric field in the vicinity of the plasmonic nanostructures. The second enhancement, known as the chemical enhancement, occurs due to the transfer of charge between the molecules and the metallic nanostructures and is typically of the order of 10^1-10^3 [3].

There are several requirements for a SERS substrate to be considered as an optimum substrate such as a large average electromagnetic field enhancement, broadband resonance spectrum, high reproducibility, and high tunability. Though it is quite challenging to achieve the above criteria in a SERS substrate simultaneously, efforts have been made recently [1,5] to improve the quality of the SERS substrates in order to meet most of the above criteria. A large number of SERS substrates have been fabricated in recent years such as island films [6,7], plasmonic nanowires [8], nanobundles [9], nanofingers on nanowires [10], nanocubes and nanoblocks [11], elevated gold ellipse nanoantenna dimers [12], gold nanorings [13], and hybrid nanoparticle-nanolines [14].

There is another class of plasmonic nanostructures known as the periodic array of nanoholes in a plasmonic thin film (such as a gold or silver thin film), and these nanostructures can also be employed as SERS substrates. When light is incident on this periodic array of nanoholes, an extra momentum is provided to the incident light by the periodicity of nanohole array. Therefore, incident light couples to surface plasmon polaritons (SPPs) on the metal-dielectric interface facing the incident light. The mechanism of extraordinary transmission through nanohole arrays in plasmonic thin films depends on the thickness of the thin film [15,16]. When the thickness of the plasmonic thin film is small, the

Optics EXPRESS

SPPs on the incident metal-dielectric interface resonantly couple to the SPPs on the exit metal-dielectric interface, leading to the formation of a surface plasmon (SP) molecule [16]. On the other hand, as the thickness of the plasmonic thin film is larger, there is a sequential process of coupling of the incoming photons into SPPs on the incident metal-dielectric interface, tunneling to the SPPs at exit interface, and coupling to the radiative mode on the exit interface [15,16]. The wavelength, at which incident field couples into SPPs at the metal-dielectric interface can be approximately given by following formula [17]:

$$\lambda = \frac{P}{\sqrt{i^2 + j^2}} \sqrt{\frac{\varepsilon_m \varepsilon_d}{\varepsilon_m + \varepsilon_d}} \tag{1}$$

where P is the period of a square array of nanohole, i and j correspond to the different modes, and ε_m and ε_d are the relative permittivities of metal and dielectric respectively. Apart from nanohole periodicity, peak wavelength in transmission spectra is also affected by shape resonance [18], LSPR effect [18,19], and waveguide modes [20].

Nanohole arrays in plasmonic thin films have been exploited for various applications including SERS-based sensing of chemical molecules [21–24], The maximum SERS enhancement factor reported thus far by employing nanohole arrays as SERS substrates is less than 10^6 [21]. Although the SERS enhancement factor in SERS substrates using nanohole arrays is significantly less than those employing plasmonic nanoantenna arrays, the area of the SERS hotspots (i.e. the regions where there is substantial SERS enhancement) is much larger in the case of nanohole arrays as compared to the nanoantenna arrays. In this paper, we present novel nanohole arrays (bridged-bowtie and cross bridged-bowtie nanohole arrays) as SERS substrates that not only exhibit large electromagnetic enhancement of SERS but also have the SERS enhancement spread over a much larger area than what could be present in SERS substrates consisting of nanopillar arrays or nanopillar plasmonic nanoantennas.

In this paper, we report a comprehensive study of nanohole arrays containing novel geometries of nanoholes such as a bridged-bowtie nanohole array and a cross bridged bowtie nanohole array (see Fig. 1). These nanohole arrays can be used, in both, the reflection mode as well as in the transmission mode. It was found that both the bridged-bowtie nanohole array and the cross bridge-bowtie nanohole array exhibit electromagnetic enhancement of SERS (electromagnetic SERS EF) of ~10^9, which is orders of magnitude higher than what has been previously reported for nanohole arrays as SERS substrates [21] and also over 3 orders of magnitude higher than that of a bowtie nanohole array. As SERS chemical enhancement factors are typically between 10^1 and 10^3, the total SERS enhancement factors provided by the SERS substrates being proposed by us can lie between 10^{10} and 10^{12}. In crossed bridged-bowtie nanohole arrays, electromagnetic SERS enhancement (of ~10^9) is spread over a hotspot region of ~100 nm^2, which is larger than the case of arrays of bowtie nanoantennas (hot spot region being ~5 nm by 5 nm for the electromagnetic enhancement of SERS being greater than 10^8 – see Appendix A). As it is very difficult for biomolecules to go inside small gaps (say sub-5 nm gaps) between nanopillars of a bow-tie nanoantenna [8,9], the nanohole array based SERS substrates described in this paper are more desirable for biosensing as biomolecules can easily reach the SERS hotspots (the corners of nanotriangles present in a bridged-bowtie nanohole array and a cross bridged bowtie nanohole array). This is because the tips of these nanotriangles are at least ~15 nm apart. Moreover, the nanostructures proposed in this paper have a very high electromagnetic SERS EF at the surface of the nanoholes, which is beneficial for biosensing [25]. In addition, it was observed that an electromagnetic SERS enhancement factor of at least 10^8 is spread over a large area (~550 nm^2) and of at least 10^7 over an area of ~1550 nm^2, thus increasing the average enhancement factor. These nanohole geometries also provide the tunability of resonance wavelength by varying the size of nanoholes. In addition, it is seen that the large electromagnetic SERS EF occurs at three wavelengths for the bowtie nanohole array and at two wavelengths for the

Optics EXPRESS

cross bridged-bowtie nanohole array. Therefore, it provides a platform to obtain multiple wavelength SERS response [26,27]. Moreover, in the cross bridged-bowtie nanohole array being presented in this paper, the position of hotspot on the SERS substrate can be tuned by varying the polarization of incident electromagnetic field. Therefore, the proposed nanohole arrays (the bridged-bowtie nanohole array and the cross bridged bowtie nanohole array) provide excellent platforms to be used as SERS substrate for chemical and biological sensing.

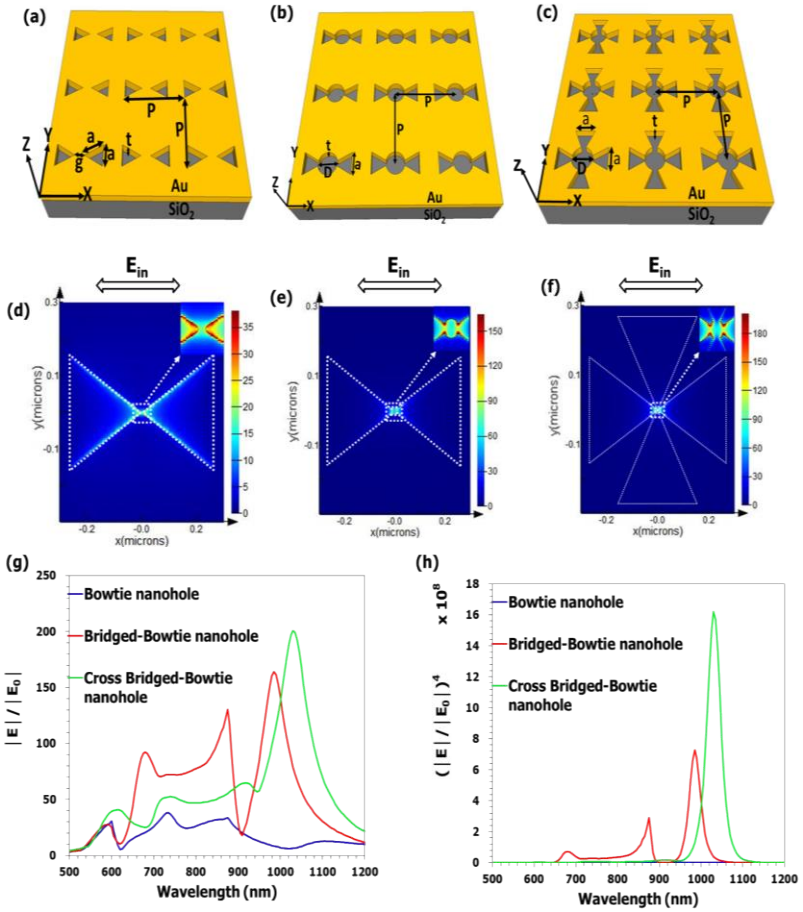

Fig. 1. Schematics of a periodic arrays of nanoholes in a gold film for the different geometries of the nanoholes: (a) bowtie nanoholes, (b) bridged-bowtie nanoholes and (c) cross bridged-bowtie nanoholes. The different parameters described in the schematics are the period 'P' of nanoholes in the nanohole array, gold film thickness 't', nanohole side dimension 'a', circular bridge hole diameter 'D', and gap between the tips of the bowtie nanoholes 'g'. A circular nanohole of diameter 'D' is employed to bridge the bowtie nanoholes and cross bowtie nanoholes to form the bridged-bowtie nanoholes and cross bridged-bowtie nanoholes, respectively. Light can be incident either from the substrate side or from the air side, and the electric field enhancement factor (EF) and SERS enhancement factor (EF) is measured at the top metal-air interface. Spatial distribution of electric field enhancement on the surface of the metal-air interface when the light is incident from the air side for: (d) a bowtie nanohole array, (e) a bridged-bowtie nanohole array, and (f) a cross bridged-bowtie nanohole array. (g) Maximum electric field enhancement factor (EF) and (h) Maximum electromagnetic enhancement of SERS (SERS EF) on the surface of the metal-air interface in nanohole arrays having three different nanohole geometries (bowtie nanoholes, bridged-bowtie nanoholes and cross bridged-bowtie nanoholes). The period (P) of nanoholes in the nanohole array was kept constant at 600 nm in (g) and (h).

Optics EXPRESS

2. Finite difference time domain simulations

To study the different nanohole array geometries, we have employed the finite difference time domain (FDTD) method. In the FDTD method, Maxwell's equations are discretized in both space and time, and the central-difference approximation is employed. A commercial FDTD software called Lumerical FDTD solution was employed in this paper to analyze the electromagnetic fields around our plasmonic nanostructures as well as to determine the reflection and transmission of light through the nanostructures. Our nanostructures consist of a gold film on a silica substrate with a periodic array of nanoholes perforated in the gold film (in the XY plane). The period 'P' of nanohole array was kept constant at P = 600 nm for all the geometries of nanoholes studied in this work. To analyze our proposed geometry in the transmission mode, the source was present on the substrate side. In the reflection mode, the source was present on the air side. Periodic boundary conditions were used in X and Y directions. PML boundary condition was applied along the Z direction to avoid any reflection from boundaries. A non-uniform mesh was used for the FDTD simulations. While a mesh size of 1 nm was taken in the gap region, a mesh size of 2 nm was taken throughout the structure in the XY plane. In the Z direction, a mesh size of 5 nm was selected. The dielectric constant of the gold film was modeled by a dispersion relation provided by Palik [28].

3. Results and discussion

In this section, we analyze and compare the results of FDTD simulations carried out on nanohole arrays having different geometries. The electromagnetic SERS enhancement factor (SERS EF) and the spatial field distribution were calculated for various geometries of nanohole arrays (both in reflection mode and the transmission mode) and the results of those simulations are presented and analyzed. Furthermore, the effect of polarization of the incident field has also been studied for bridged-bowtie nanohole and the cross bridged-bowtie nanohole array. Moreover, we study the effect of thickness of the gold film and the diameter of bridge-nanohole (i.e. the circular nanohole bridging the bowtie nanoholes).

Figure 2 presents results of FDTD simulations showing the electromagnetic SERS EF as a function of wavelength for bowtie nanohole array, bridged-bowtie nanohole array and cross bridged-bowtie nanohole array in transmission mode as well as in reflection mode for different sizes of nanoholes present in the array. It can be observed from Fig. 2(a) and Fig. 2(d) that for an array of bowtie nanoholes, the electromagnetic SERS EF attains a maximum value ~3.3 x 10^5 at a wavelength of 600 nm in transmission mode for hole size 'a' = 300 nm. In the reflection mode, the array of bowtie nanoholes have a maximum electromagnetic SERS EF of ~10^7 at a wavelength of 705 nm when the hole size 'a' = 200 nm. This electric field enhancement as well as the extraordinary transmission through the nanohole array (as described in Appendix B) are caused at the both the metal-dielectric interfaces by the excitation of surface plasmon resonance (SPR) at the metal-dielectric interfaces [29]. This is also explained earlier by Brolo et al. [21] for a nanohole array containing circular nanoholes. While both the electric field enhancement at the metal-dielectric interfaces and the extraordinary transmission through nanohole array depend on the complex phenomenon involving coupling of the incident radiation into SPPs on the metal-dielectric interfaces, the enhancement of the electric fields on the metal-dielectric interfaces also depends on other factors such as the geometry of the nanoholes and the arrangement of nanoholes (which will determine the localized electric fields on the surface of the metal-dielectric interfaces [30]).

Moreover, the electromagnetic SERS EF also increase with the size of bowtie nanoholes present in the array as shown in Figs. 2(a). An increase of the size of the nanoholes in a nanohole array leads to a stronger increase in transmission (as shown in Appendix B), than might have been expected based on conventional aperture theory, as the nanoholes mediate the coupling between the surface plasmon polaritons on the two metal-dielectric interfaces — with the larger holes leading to a larger coupling [31,32]. Increase in the transmission with the

Optics EXPRESS

size of the bowtie nanoholes in turn results in a higher electromagnetic SERS EF in transmission mode.

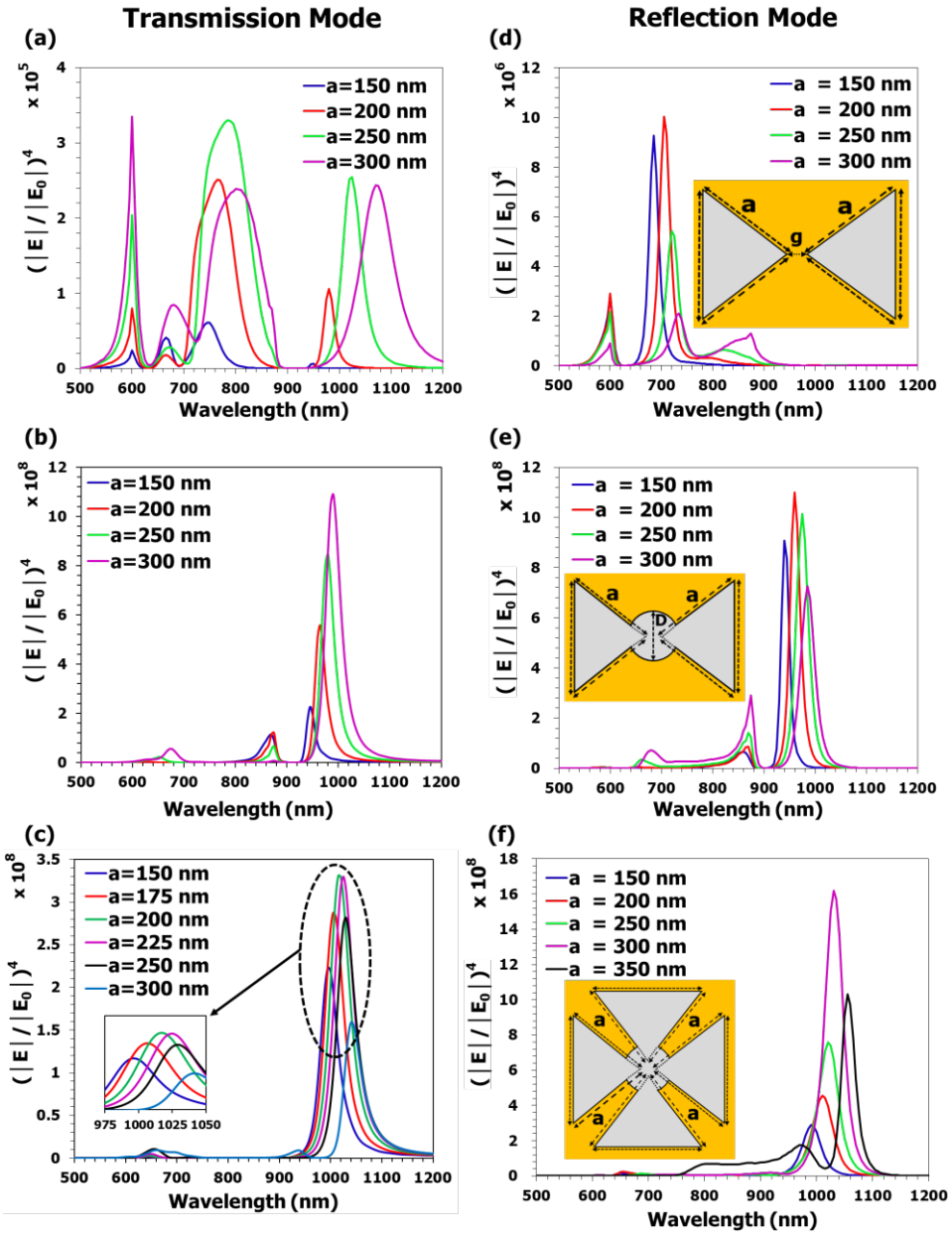

Fig. 2. Electromagnetic SERS enhancement factor in transmission mode configuration (left column) for (a) bowtie nanoholes, (b) bridged-bowtie nanoholes and (c) cross bridged-bowtie nanoholes arrays. The light is incident from the substrate side and electromagnetic enhancement factor was measured at surface of the metal-air interface. Electromagnetic SERS enhancement factor in reflection mode measurement for (d) bowtie nanoholes, (e) bridged-bowtie nanoholes and (f) Cross bridged-bowtie nanoholes array. In reflection mode configuration, light is incident from the substrate side and electromagnetic SERS EF factor was measured at surface of the metal-air interface. The side dimension 'a' of the nanoholes was varied from 150 nm to 250 nm, while the nanohole period 'P', the gap between the tips of the bowtie nanoholes 'g' and the thickness of the gold film 't' were kept constant at 600 nm and 10 nm, and 200 nm respectively. Figures in the inset are not to the actual scale.

Optics EXPRESS

In addition, as the size of the nanohole increases, electromagnetic SERS enhancement has a red shift in the wavelength as shown in the Fig. 2(a). As the hole width is decreased, the resulting decrease in transmission will be less for shorter wavelengths than for larger wavelengths, as the transmission beyond cutoff has a nonlinear dependence on wavelength. This effectively leads to a blue-shift as the hole size is decreased, which means there is a red-shift as the hole size is increased [31].

Figures 2(b) and 2(e) show the electromagnetic SERS EF spectra in transmission mode and in reflection mode, respectively, for the bridged-bowtie nanohole array. In a bridged-bowtie nanohole array, a circular nanohole, of diameter 20 nm, is employed to bridge the bowtie nanoholes and form each 'bridged-bowtie' nanohole. The process of bridging the bowtie nanoholes forms sharp corners in the nanohole geometry, thereby leading to high electric field enhancement in the regions between neighboring corners, and therefore high electromagnetic enhancement of SERS in substrates containing these nanostructures. It can be observed from Fig. 2(b) that extremely large electromagnetic SERS EF were obtained at several wavelengths — 680 nm, 870 nm, and 990 nm, for the hole size 'a' of 300 nm in the transmission mode. These peaks correspond to the different SPR orders at metal-substrate and metal-air interface. The highest electromagnetic enhancement factor obtained for bridged-bowtie nanohole in the transmission mode was approximately 1.0×10^9 at 990 nm for a hole size of 300 nm. Figure 2(e) shows the electromagnetic SERS enhancement factor spectra for the bridged-bowtie nanohole array for the reflection mode configuration, and it was observed that the highest electromagnetic enhancement of SERS for this nanohole array was approximately 1.1×10^9 at a wavelength of 960 nm and 9.4×10^7 at 885 nm for hole size 'a' = 200 nm. These extremely large electromagnetic SERS enhancement factors at multiple wavelengths for a bridged bowtie nanohole array can be exploited for multiple wavelength SERS response [26,27].

The effect of size of the bridged-bowtie nanoholes on the electromagnetic SERS EF is shown in Fig. 2(b) and Fig. 2(c) for the transmission mode and the reflection mode, respectively. It can be seen that for the transmission mode, the electromagnetic SERS EF increases as the size of the bowtie nanohole is made bigger. The larger sized nanoholes allow better coupling between the SPPs on the two metal-dielectric interfaces (the metal-substrate interface and the metal-air interface). On the other hand, for reflection mode the electromagnetic SERS EF attains an optimum value for hole size "a" = 200 nm and starts decreasing for larger hole size. The decrease in electromagnetic SERS enhancement factor for very large nanohole sizes can be attributed to these nanoholes supporting propagative modes, which do not contribute to the electric field enhancement in the reflection mode. Furthermore, there is a red-shift in the electromagnetic SERS EF spectrum with an increase in the nanohole size, as was observed in the case of bowtie nanohole arrays.

It can be observed from Fig. 2(a) and 2(b) that bridged-bowtie nanohole arrays show extremely large enhancement factors as compared to bowtie nanohole array. The extremely large enhancement factors in bridged-bowtie nanohole array can be attributed to the two effects. The first effect is the coupling of the incident optical fields to the SPPs at the metal-substrate interface and the metal-air interface, thereby leading large electric field enhancements at the metal-air interface. Secondly, the bridged-bowtie nanohole structure comprises of two sets of two pointed nanotriangles facing each other (forming bowtie nanopillar like structures) leading to high electric field enhancements between at the corners of these nanotriangles (See Fig. 3). This very high electric field enhancement factor (EF) can be attributed to the coupling of the incident light to LSPs in the nanotriangles facing each other (formed due to the bridging of the two triangular nanoholes forming a bowtie nanohole), as well as to the lightening rod effect, which occurs due to the sharp metallic corners of these nanotriangles.

Figure 2(c) presents another geometry of the nanoholes—cross bridged-bowtie nanoholes—forming an array on a gold thin film. Figures 2(c) and 2(f) show the

Optics EXPRESS

electromagnetic SERS EF spectra, for transmission mode configuration and the reflection mode configuration respectively, for a cross bridged-bowtie nanohole array. It can be observed from Fig. 2(c) that the qualitative behavior of the spectra for electric field enhancement factor is same as that for a bridged-bowtie nanohole array, except for the fact that the highest electric field EF has an optimum value as a function of the size 'a' of the nanohole. Initially, an increase in the size of the cross bridged-bowtie nanohole leads to better coupling of the SPP modes at the metal-dielectric interfaces. Therefore it results in an increase in the electric field EF. As the size of the cross bridged-bowtie nanohole is further increased, these nanoholes starts supporting propagative modes, which do not contribute to the electric field enhancement. As a result, a maximum value of electromagnetic SERS EF is obtained for the cross bridged-bowtie nanohole array for an optimum nanohole size 'a' of 200 nm. Furthermore, while multiple peaks are observed in the electric field EF spectra (shown in Fig. 2(c), significant electromagnetic SERS enhancement (i.e. greater than 10^7) occurs primarily at wavelengths of ~660 nm and ~1015 nm (as shown in Fig. 2(c)). The maximum value of electromagnetic SERS enhancement factor, for a 200 nm of nanohole size, was calculated to be 3.3 x 10^8 at a wavelength of 1015 nm, as shown in Fig. 2(c). Figure 2(f) shows the electromagnetic SERS EF for cross bridged-bowtie nanohole array for reflection mode configuration. The maximum electromagnetic SERS enhancement factor obtained for reflection mode configuration was approximately 1.6 x 10^9 at a wavelength of 1030 nm. This is substantially larger than the electromagnetic SERS enhancement factor obtained for an array of gold bowtie nanoantennas (see Appendix A), for an array of gold nanorod antennas (see Appendix C), and for an array of circular nanoholes (see Appendix D).

It can be observed from Fig. 2 that the electric field EF attains a higher value in the reflection mode as compared to that obtained in the transmission mode for a crossed bridged-bowtie nanohole array. For the cross bridged-bowtie nanoholes array, the highest electromagnetic enhancement factor when obtained in reflection mode is ~1.6 x 10^9 at a wavelength of 1030 nm (for a nanohole size 'a' = 300 nm and gold film thickness 't' = 200 nm). This is higher than the highest electromagnetic enhancement of SERS for this nanohole array obtained in the transmission mode (~3.3 × 10^8), as shown in Fig. 2(c). In the transmission mode, some energy is lost in the transmission process through the metallic thin film containing the arrays of nanoholes, leading to a slightly lower electric field EF in the transmission mode. Obtaining high values of electric field EF and electromagnetic SERS EF in the reflection mode is important, as the SERS substrates are primarily employed in the reflection mode.

Figure 3 shows the spatial distribution of the electric field enhancement (at resonance wavelength) for different geometries, for bowtie nanohole array, bridged-bowtie nanohole array, and cross bridged-bowtie nanohole array reflection mode configuration. It can be observed from Fig. 3(b) and 3(c) that for bridged-bowtie and cross bridged-bowtie nanohole array, the electric field is enhanced at the corners (sharp nanotriangle pairs) that were formed in the process of bridging the bowtie nanoholes as explained above. Moreover, for the bridged-bowtie nanoholes structure being proposed in this paper, it is observed that there is a much larger area over which the hotspot is observed as compared to a conventional bowtie nanoantenna (based on two triangular nanopillars), wherein the hotspot length generally is less than 5 nm by 5 nm (for electromagnetic SERS enhancement factors greater than 10^8 – see Appendix A). In the case of the bridged-bowtie nanohole arrays, it is also observed that the hotspot is not just limited to the tips of the bowtie nanopillars formed due to the formation of the bridge between the bowtie nanoholes (where the highest electromagnetic SERS enhancement is ~10^9), and a significant electromagnetic SERS enhancement factor of ~10^7 is present over a region of ~1500 nm^2 in each periodic unit of the array (and of ~10^8 is present over a region of ~500 nm^2), thus increasing the average enhancement factor. It has to be noted that size of each periodic unit in the nanohole array is 600 nm by 600 nm. For cross bridged-bowtie nanohole array exhibits a highest electromagnetic SERS enhancement factor (EF) of

Optics EXPRESS

~10^9 spread over a hotspot area ~100 nm^2 (in each periodic unit of the array), which is larger than the case of arrays of bowtie nanoantennas (hot spot region being ~5 nm by 5 nm for the electromagnetic enhancement of SERS being greater than 10^8—see Appendix A). In addition, it can be observed from Fig. 3(c) that an electromagnetic SERS enhancement factor of at least 10^8 is spread over an area ~550 nm^2, and 10^7 being present over a hotspot area of ~1550 nm^2, thus increasing the average enhancement factor. As SERS chemical enhancement factors are typically between 10^1 and 10^3, the highest overall SERS enhancement factors provided by the SERS substrates being proposed by us can lie between 10^{10} and 10^{12}. It has to be noted that the highest SERS enhancement factors reported previously for controllably fabricated SERS substrates lie between 10^9 and 10^{12} [33,34]. Hence, the SERS substrates being proposed by us (based on bridged-bowtie nanohole arrays) not only have a very high SERS enhancement factor but also have the SERS enhancement spread over a larger area than what could be present in SERS substrates consisting of nanopillars or plasmonic nanoantennas.

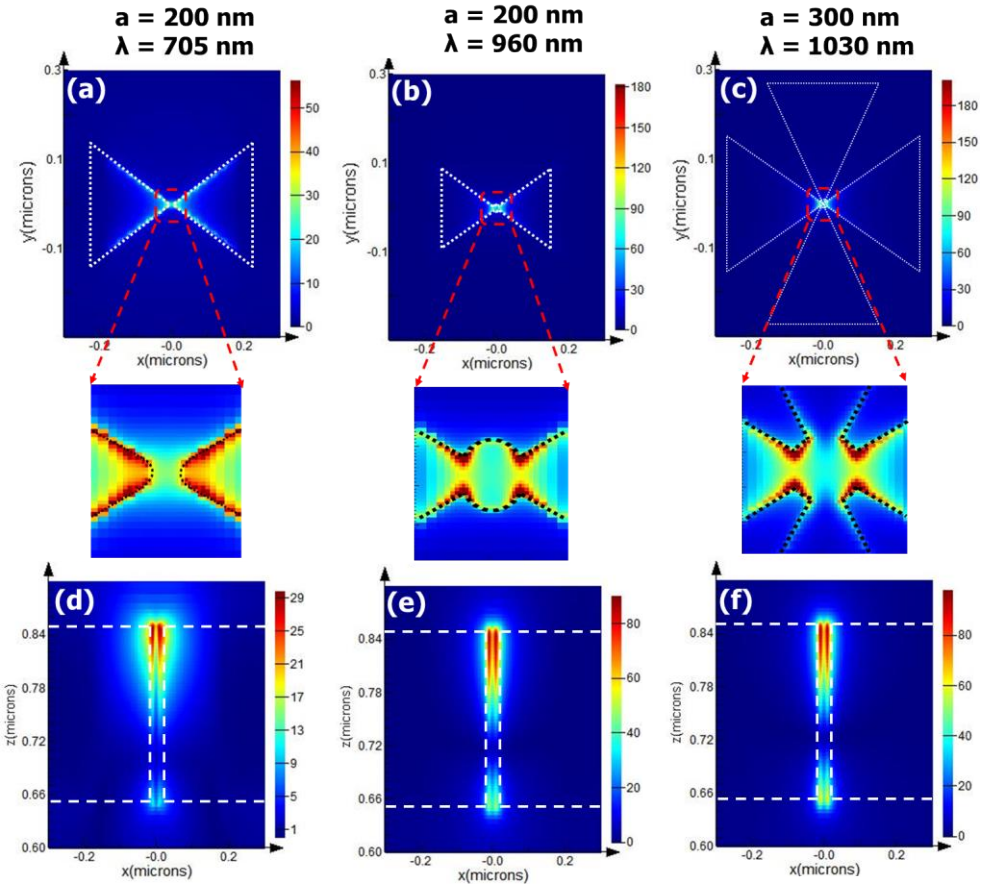

Fig. 3. Spatial distribution of electric field enhancement on the surface of a metal-dielectric interface (in the XY plane) in a periodic array of (a) bowtie nanoholes, (b) bridged-bowtie nanoholes, and (c) cross bridged-bowtie nanoholes present in a gold film of thickness 't' = 200 nm in reflection mode configuration. (a) Nanohole side dimension 'a' = 200 nm at 705 nm wavelength of the incident light, (b) 'a' = 200 nm at 960 nm wavelength, and (c) 'a' = 300 nm at 1030 nm wavelength. The nanohole period 'P' and the circular bridge hole diameter 'D' were kept constant at 600 nm and 20 nm, respectively. (d-f) Spatial distribution of the electric field enhancements in the XZ plane for the three different geometries of nanohole array: (d) bowtie nanohole array (e) bridged-bowtie nanohole array (f) crossed bridged-bowtie nanohole array. The incident field was polarized along Y axis. Light was incident from the air side, and the electric field enhancement was measured at the top metal-air interface.

Optics EXPRESS

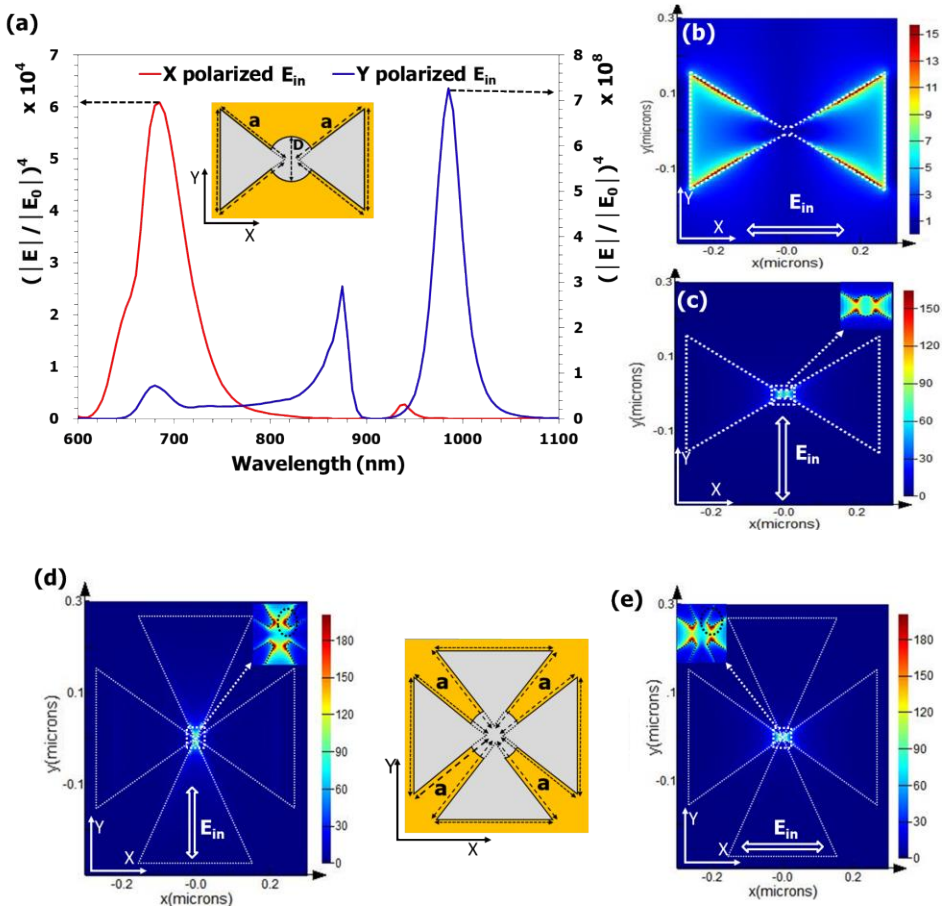

Fig. 4. (a) Comparison of the electromagnetic SERS enhancement factor when the incident electric field is polarized along the Y direction (blue curve) and X direction (red curve) in a bridged-bowtie nanohole array. Comparison of the spatial distribution of the electric field enhancement when the incident electric field is polarized along the (b) X axis and (c) Y axis in bridged-bowtie nanohole array. Comparison of the spatial distribution of the electric field enhancement when the incident electric field is polarized along the (d) Y axis and (e) X axis in a cross bridged-bowtie nanohole array. Light was incident from the air side, and the electric field enhancement was measured at the top metal-air interface in a periodic array of bridged-bowtie nanoholes of side 'a' = 300 nm present in a gold film of thickness 't' = 200 nm. The nanohole period 'P' and the circular bridge hole diameter 'D' were kept constant at 600 nm and 20 nm, respectively.

Figure 4 shows the effect of polarization on bridged-bowtie nanohole and cross bridged-bowtie nanohole array in reflection mode configuration. It was observed that electromagnetic SERS EF drastically decreases from ~10^8 to ~10^4 as the polarization of the incident electric field was rotated from Y to X-axis. This can be explained primarily on the basis of the formation of two nanotriangle pillars facing each other in the Y-direction (forming two bowtie nanopillar like structures) when we bridge the two triangular nanoholes forming a bowtie nanohole with a circular nanohole. When the polarization of the incident field is in the Y-direction, it leads to very large enhancement of electric fields (as shown in Fig. 4(c)) at the tips of these nanotriangle pillar pairs. This is due to the orientation of the dipoles in the nanotriangle pairs along the direction of the incident electric field (i.e. the Y-direction). Moreover, when the incident field is polarized along the Y-axis, maximum electric field enhancement occurs at larger wavelengths. However, when the incident field is polarized along X-axis, maximum electric field EF occurs at relatively shorter wavelength (as shown in

Optics EXPRESS

Fig. 4(a)). This can be attributed to the cut-off function of the bridged-bowtie nanohole forming the array. Since dimensions of the nanoholes are different in Y and X direction, there exist two cut-off functions corresponding to the two orthogonal axis. As the direction of polarization of incident field is rotated from Y to X-axis, it changes the position of LSP modes as well as the cut-off function of nanohole array [19]. A distinction in the field profile (spatial distribution of the electric field enhancement) is also observed for the two orthogonal states of polarization as shown in Figs. 4(b) and 4(c).

Figure 4(d) and 4(e) shows how the position of the hotspots can be shifted by rotating the direction of the polarization of the electric field incident on the cross bridged-bowtie nanohole array. When the incident field is polarized along the Y-axis, the field is enhanced at the corners that are closer to the X-axis and vice versa. Therefore, as the direction of the incident field is rotated from Y to X direction, the hotspots shift to adjacent corner. This allows tunability of position of the hotspot (on a SERS substrate) by changing the direction of polarization of the incident beam. It has to be noted that the highest electric field EF as well as the area over which the hotspot is present are significantly large for both the X and the Y polarizations of light incident on the cross bridged-bowtie nanohole array.

Figure 5 shows the effect of film thickness 't' and the diameter 'D' of a circular nanohole (the bridge nanohole) for a cross bridged-bowtie nanohole array. It can be observed from Fig. 5(a) that electromagnetic SERS EF decreases with an increase in the film thickness and the peak wavelength also undergoes a significant red-shift. At longer wavelengths, penetration depth of SPPs into the metal become significantly large, thereby, allowing the coupling of SPP modes at the two interfaces (metal-substrate interface and the metal-air interface). Hence, in the cross bridged-bowtie nanohole array structure being presented in our paper, increasing the thickness of the metal layer from 175 nm to 250 nm leads to lower transmission through the nanoholes as the transmission mechanism is based on evanescent transmission through the nanoholes (i.e. transmission when there is no coupling between the SPPs on the two interfaces of the metal-dielectric interfaces). This results in a decrease in the electric field enhancement and therefore in the electromagnetic SERS EF. As the film thickness is decreased below 175 nm, there is coupling between the SPPs on the two interfaces of the metal-dielectric interfaces, leading to the existence of two non-degenerate modes [35] – with the mode at a higher wavelength having a lower electric field enhancement and therefore a lower electromagnetic SERS EF.

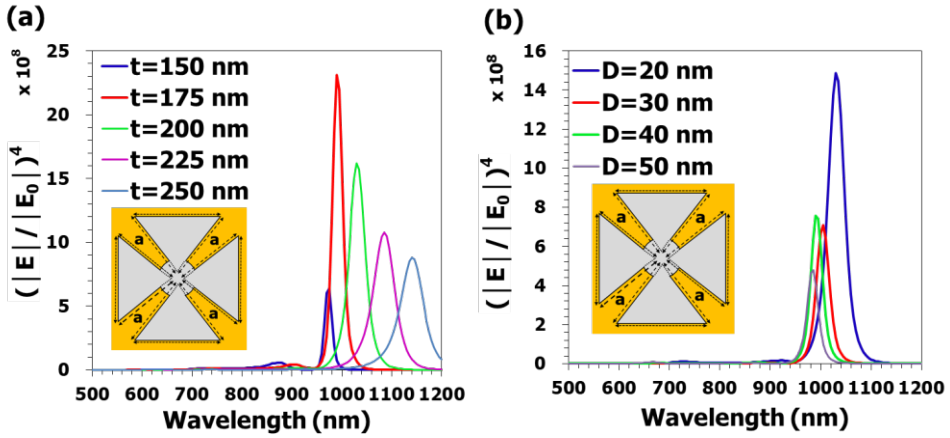

Fig. 5. The effect of (a) Gold film thickness 't' and (b) Diameter 'D' of circular bridge nanohole on the electric field enhancement factor (EF) spectra for a cross bridged-bowtie nanohole array. In (a) the diameter of circular bridge hole was taken as 20 nm and in (b) the thickness of the gold film was taken as 200 nm. The nanohole period 'P' was kept constant at 600 nm. Light was incident from the substrate side and the electric field enhancement factor was measured at the top metal-air interface. The incident electric field was polarized along Y axis.

Optics EXPRESS

Figure 5(b) shows the effect of the radius of the cross bridged-bowtie nanohole on the electromagnetic SERS EF. It can be observed from Fig. 5(b) that the electromagnetic SERS EF decreases as the radius of the nanohole increases. As the radius of the cross bridged bowtie nanohole increases, the distance between the sharp corners of the triangular nanopillars (formed as a result of the cross bridged-bowtie nanohole) becomes large, leading to a reduction in the electric field enhancement between the triangular nanopillars.

The nanohole arrays described in this paper can be fabricated by first employing electron beam deposition to deposit gold thin films on silica substrates, and then employing one of the nanolithography processes such as focused ion beam milling (using either a helium ion beam [36,37] or a gallium ion beam [38]), Transmission Electron Beam Ablation Lithography [40], or a combination of these processes. In order to fabricate the bridged-bowtie nanostructures by employing FIB milling (using a helium ion beam), we can employ a two-step fabrication process: the first step involving fabrication of a bowtie nanohole antenna using FIB milling and a second step involving FIB milling of a circular hole from the middle the triangular nanoholes forming the bowtie nanohole antenna. Moreover, electron beam lithography (e.g. using a negative photoresist [39]), followed by metal deposition and lift-off can be employed for fabrication the nanohole arrays described in this paper.

4. Conclusions

In conclusion, bridged-bowtie nanohole arrays and cross bridged-bowtie nanohole arrays were studied using FDTD numerical simulations, and it was found that both bridged-bowtie nanohole arrays and the cross bridged-bowtie nanohole arrays exhibit large electromagnetic SERS enhancement factors and therefore provide excellent platforms to be used as SERS substrates. It was observed that the bridged-bowtie nanohole array and the cross bridge-bowtie nanohole array exhibit an highest electromagnetic SERS enhancement factor (EF) of ~10^9, which is orders of magnitude higher than what has been previously reported for nanohole arrays as SERS substrates. This electromagnetic SERS EF (of ~10^9) is spread over a hotspot region of ~100 nm^2, which is larger than the case of nanopillar arrays. In addition, it was observed that an electromagnetic SERS enhancement factor of at least 10^8 is spread over a large area (500 nm^2 in each periodic unit of the array) and of at least 10^7 over a larger area (1550 nm^2 in each periodic unit of the array), thus increasing the average enhancement factor. Study of polarization showed that bridged-bowtie nanohole arrays exhibit polarization anisotropy and provide high values of electromagnetic SERS EF only when the incident electric field is polarized perpendicular to the axis of the nanoholes. On the other hand, the cross bridged-bowtie nanohole arrays exhibit high values of electromagnetic SERS EF in both the cases when the incident electric field is polarized parallel or perpendicular to the axis of the nanoholes. It was also observed that position of the hotspots on the SERS substrates can be varied by rotating the direction of the polarization of the electric field incident on the cross bridged-bowtie nanohole arrays. High electric field enhancement factors (EFs) and electromagnetic SERS EFs were obtained for light being incident on the nanohole arrays from both the metal-substrate interface side and the metal-air interface side. This implies that the bridged-bowtie nanohole arrays and the cross bridged-bowtie nanohole arrays can be employed as effective SERS substrates in both the transmission mode and the reflection mode. The resonance wavelength of these arrays of nanoholes can be tuned by altering the size of the nanoholes. Moreover, bridged-bowtie nanohole arrays and cross bridged-bowtie nanohole arrays exhibit very high electric field enhancement factor (EF) at more than one wavelength, and therefore, can be used to obtain a multiple wavelength SERS response. Hence, the SERS substrates being proposed by us (based on bridged-bowtie nanohole arrays and cross bridged-bowtie nanohole arrays) not only have a very high electromagnetic SERS enhancement factor but also have the electromagnetic SERS enhancement spread over a larger area than what could be present in SERS substrates consisting of nanopillars or plasmonic nanoantennas.

Optics EXPRESS

Appendix A: Electromagnetic SERS EF in a 2-D periodic array of gold bowtie nanoantennas

The highest electromagnetic SERS EF was calculated for a 2-D periodic array of gold bowtie nanoantennas (i.e. triangular shaped gold nanopillars forming the bowtie antennas) as shown in Fig. 6. The period of bowtie nanoantenna array was taken 600 nm in both x and y directions. We can observe from Fig. 6 that the Electromagnetic SERS EF is only ~ 1.1×10^6 for a 2-D periodic array of gold bowtie nanoantennas, when the gap between the nanotriangles forming the bowtie nanoantenna is 20 nm. Even when the spacing between the triangles forming the bowtie nanoantenna is 10 nm, the Electromagnetic SERS EF is only ~ 9.6×10^6 (as shown in Fig. 6(a)). Moreover, even when the spacing between the nanotriangles forming the bowtie nanoantenna is 5 nm, the Electromagnetic SERS EF is only ~ 5.5×10^8 (as shown in Fig. 6(b)).

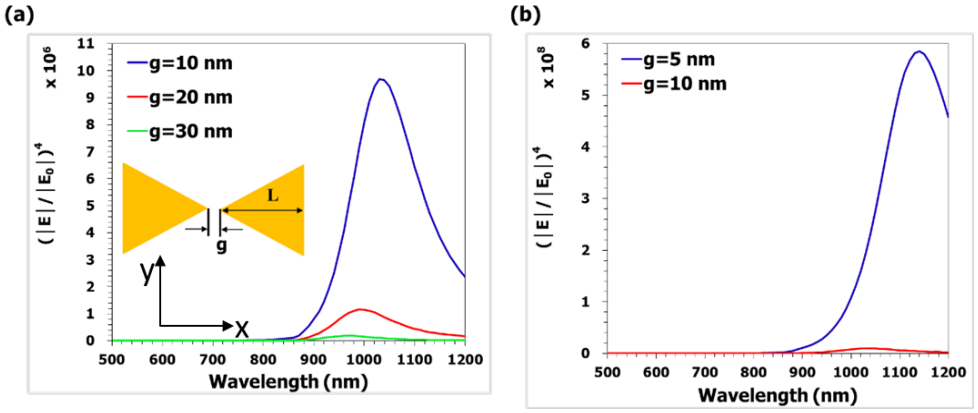

Fig. 6. Electromagnetic SERS EF in the periodic array of gold bowtie nanoantennas as a function of gap 'g' between the nanotriangles forming the bowtie nanoantenna. The length 'L' of each nanotriangle forming the bowtie nanoantenna was taken as 200 nm and the apex angle of the nanotriangle was taken to be 60 degrees. The period of bowtie nanoantenna array was taken 600 nm. The Electromagnetic SERS EF is shown for (a) Gaps 'g' ranging from 10 nm to 30 nm and for (b) Gaps 'g' ranging from 5 nm to 10 nm.

Appendix B: Extraordinary transmission spectra for bowtie nanoholes, bridged-bowtie nanoholes, and cross bridged-bowtie nanoholes arrays

It can be observed from Fig. 7 that there are peaks in the extraordinary transmission spectra for arrays of bowtie nanoholes, bridged-bowtie nanoholes and cross bridged-bowtie nanoholes. It can also be observed from Fig. 2(a)-2(c) that a high electric field enhancement occurs at wavelengths where there is a peak in the extraordinary transmission spectra shown in Fig. 7. This happens because both the extraordinary transmission through nanohole array as well as the electric field enhancement at the metal-dielectric interfaces are caused by the excitation of surface plasmon resonance (SPR) at the metal-dielectric interfaces [34]. This is also explained earlier by Brolo et al. [25] for a nanohole array containing circular nanoholes. While both the extraordinary transmission through nanohole array and the enhancement in the electric fields at the metal-dielectric interfaces depend on the complex phenomenon involving coupling of the incident radiation into SPPs on the metal-dielectric interfaces, the enhancement of the electric fields on the second metal-dielectric interface also depends on other factors such as the geometry of the nanoholes and the arrangement of nanoholes (which will determine the localized electric fields on the surface of the second metal-dielectric interface [35]).

Optics EXPRESS

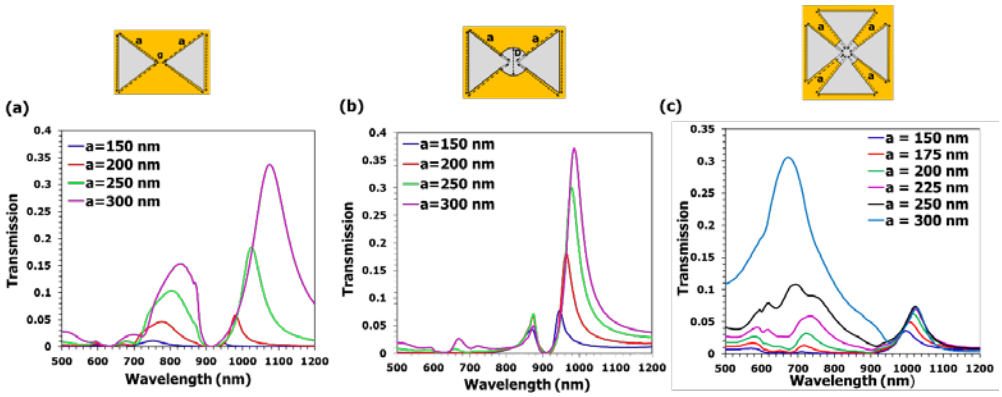

Fig. 7. The extraordinary transmission spectra for (a) bowtie nanoholes, (b) bridged-bowtie nanoholes and (c) cross bridged-bowtie nanoholes arrays. The light is incident from the substrate side. The side dimension 'a' of the nanoholes was varied from 150 nm to 250 nm, while the nanohole period 'P', the gap between the tips of the bowtie nanoholes 'g' and the thickness of the gold film 't' were kept constant at 600 nm and 10 nm, and 200 nm respectively.

Appendix C: Electromagnetic SERS EF in a 2-D periodic array of gold nanorod antennas

The highest electromagnetic SERS EF was calculated for a 2-D periodic array of gold nanorod antennas as shown in Fig. 8. We can observe from Fig. 8(a) that the Electromagnetic SERS EF is only ~ 8×10^5 for a 2-D periodic array of gold nanorod antennas, when the gap between the nanorods forming the nanoantenna is 20 nm. Even when the spacing between the nanorods forming the nanoantenna is 10 nm, the Electromagnetic SERS EF is only ~ 4.2×10^6. Moreover, even when the spacing between the nanorods forming the nanoantenna is 5 nm, the Electromagnetic SERS EF is only ~ 3.5×10^7 (as shown in Fig. 8(b)).

We can observe from Fig. 8(c) that the Electromagnetic SERS EF is only ~ 3.5×10^2 for a 2-D periodic array of gold nanorod antennas (with a minimum spacing of 10 nm between the nanorods). Even if ~ 30 such nanoantenna pairs come inside a 600 nm by 600 nm periodic region (as taken for our nanohole structures), the integrated enhancement would be 30 times 3.5×10^2, which is only ~ 1.05×10^4. Hence, the SERS substrates described in this paper (with bridged and cross-bridged nanohole arrays) provide higher theoretical EM enhancement of SERS when compared to a series of nanogap structures. Please note that we have calculated the electromagnetic SERS EFs only till 1200 nm as SERS measurements are not generally carried out at wavelengths above 1200 nm (as the Raman signals are inversely proportional to the fourth power of the wavelength on the incident light).

Appendix D: Electromagnetic SERS EF in a periodic array of circular nanoholes

We carried out FDTD simulations of arrays of circular nanoholes, so that we can compare the results for our bridged-bowtie and cross bridged-bowtie nanostructures with only the FDTD simulations for circular nanohole arrays – see results shown in Fig. 9. In the FDTD simulations, light was incident from the top surface of the metal-air interface and the Electromagnetic SERS EF was calculated in reflection mode (i.e. on the top surface of the metal-air interface itself). As it can be seen from Fig. 9, the maximum electromagnetic SERS EF is only 10^5 for the case of arrays of circular nanoholes as compared to an electromagnetic SERS EF of 10^9 for the case of bridged-bowtie and cross bridged-bowtie nanostructures being described in our paper.

Optics EXPRESS

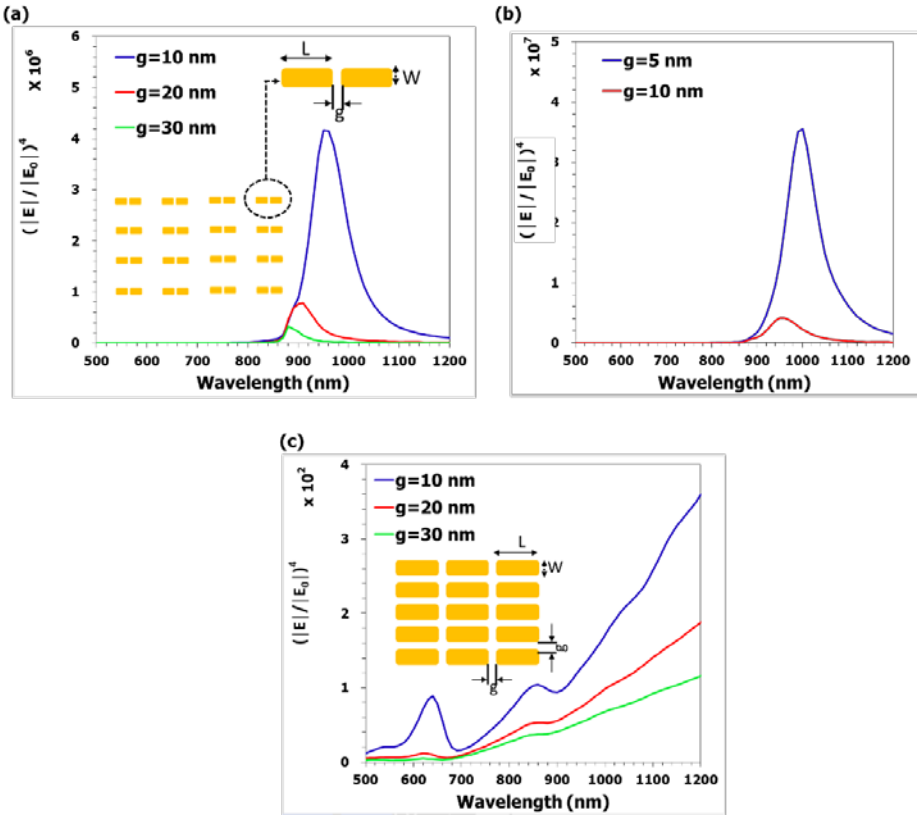

Fig. 8. Electromagnetic SERS EF in the periodic array of gold nanorod antennas as a function of gap 'g'. The length 'L' and width 'W' was chosen as 150 nm and 50 nm respectively. The Period of nanorod antenna array was taken to be 600nm. The Electromagnetic SERS EF is shown for (a) Gaps 'g' ranging from 10 nm to 30 nm and for (b) Gaps 'g' ranging from 5 nm to 10 nm. (c) Electromagnetic SERS EF in the periodic array of gold nanorod as a function of gap 'g'. The length 'L' and width 'W' was chosen as 150 nm and 50 nm respectively. The height of the nanorod was taken as 80nm.

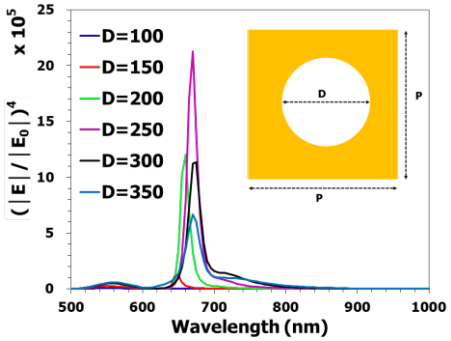

Fig. 9. Electromagnetic SERS EF in a periodic array of circular nanoholes, calculated as a function of nanohole diameter 'D'. The Period of nanohole array was taken to be 600 nm. The thickness of the gold film 't' and the period of the nanohole array was taken to be 200 nm and 600 nm, respectively. The light was incident from the top surface of the metal-air interface and the Electromagnetic SERS EF was calculated in reflection mode (i.e. on the top surface of the metal-air interface itself).

Optics EXPRESS

Funding

Government of India's Ministry of Human Resource Development (RP03246G: UAY program and RP03417G: IMPRINT program); Defense Research and Development Organization (RP03356G); Ministry of Shipping (RP03162G); Department of Science & Technology (RP03055G); and Department of Biotechnology (RP02829G, RP03150G).